Real-time electrochemical monitoring sensor for pollutant degradation through galvanic cell system

Wu-Xiang Zhang, Zi-Han Li, Rong-Sheng Xiao, Xin-Gang Wang, Hong-Liang Dai, Sheng Tang, Jian-Zhong Zheng, Ming Yang, Sai-Sai Yuan

[a] School of Environmental and Chemical Engineering, Jiangsu University of Science and Technology, Zhenjiang, 212003, P. R. China

[b]Department of Applied Physics, The Hong Kong Polytechnic University, Hongkong, SAR, 610051 P. R. China

*Corresponding author: Dr. Wuxiang Zhang, email: WXZ133@just.edu.cn

Abstract: Here, a novel real-time monitoring sensor that integrates the oxidation of peroxymonosulfate (PMS) and the in situ monitoring of the pollutant degradation process is proposed. Briefly, FeCo@carbon fiber (FeCo@CF) was utilized as the anode electrode, while graphite rods served as the cathode electrode in assembling the galvanic cell. The FeCo@CF electrode exhibited rapid reactivity with PMS, generating reactive oxygen species that efficiently degrade organic pollutants. The degradation experiments indicate that complete bisphenol A (BPA) degradation was achieved within 10 min under optimal conditions. The real-time electrochemical signal was measured in time during the catalytic reaction, and a linear relationship between BPA concentration and the real-time charge (Q) was confirmed by the equation $\ln(C_0/C) = 4.393Q$ (correlation coefficients, $R^2 = 0.998$). Furthermore, experiments conducted with aureomycin and tetracycline further validated the effectiveness of the monitoring sensor. First-principles investigation confirmed the superior adsorption energy and improved electron transfer in FeCo@CF. The integration of pollutant degradation with in situ monitoring of catalytic reactions offers promising prospects for expanding the scope of the monitoring of catalytic processes and making significant contributions to environmental purification.

Introduction

The rapid development of industry and agriculture has greatly improved the living standard of human beings, but it has also caused a series of problems such as water pollution. Advanced oxidation techniques (AOPs), , including reverse osmosis, catalysis, membrane filtration, *etc.*, can achieve water purification with high efficiency and good repeatability. The Fenton reagents in AOPs can be activated by heterogeneous catalysts and affect the degradation efficiency of organic pollutant. This technology has attracted great interest in recent years for the treatment of organic pollutants. However, catalysts with only catalytic properties do not fully meet the current transformative market demand. In many scenarios, timely monitoring the concentration of organic pollutants in water is necessary.

Traditional methods for measuring environmental organic pollutants include chromatography and spectroscopy, which have been successfully applied in medical, scientific and analytical fields. However, the solutions being measured are usually collected in a centralized manner and need to be further separated and purified, which is a tedious process. Moreover, the instruments are bulky, and costly, and require advanced operational skills that limit their practical applications. In recent years, electrochemical methods have gained extensive application and continuous improvement, while their miniaturization, rapidity, convenience, high sensitivity and easy automation provide conditions for simultaneous assays and determination in specific water environments. All these years, burgeoning electrochemical analytical methods are continuously enriched and expanded, especially in the construction of sensor methodologies based on electrochemical-related principles.

Zeolite imidazole frameworks (ZIFs), a subclass of the metal-organic frameworks, are innovative platforms for the construction of porous functional and sensor materials due to their high active site exposure and tunable precursors of transition metals (e.g., Fe, Co, Ni, Mn, Zn, etc.). To date, several admirable preparation strategies, including element replacement methods, confinement cladding, ion exchange, etching, etc. have been developed for tuning the composition and structure of bimetallic ZIFs. However, previous reports have focused more on the structure-property relationships between

functionalized features and their specific active sites, as well as their application as catalysts or sensors in specific fields. To best our knowledge, there are no reports on the removal of organic pollutants and the accurate monitoring of degradation in real time by in situ measurement techniques.

Considering that the catalyst can rapidly perform redox reactions with PMS to produce oxidatively active species that act on organic pollutants and effectively degrade them. Herein, a primary cell system with ZIFs derivative FeCo@CF as the negative electrode and graphite rod as the positive electrode was set up to measure the current generated in situ during the degradation of salt-containing wastewaters. The relevant mechanism is shown in Fig. 1. The real-time charge (Q) is calculated from the in situ measured current density by Faraday's equation ($Q = zF\xi$, F is Faraday's constant), and a good corresponding relationship to the actual measured BPA, aureomycin and tetracycline are calculated as $\ln(C_0/C) = 4.3925Q$, ($R^2=0.9987$), $\ln(C_0/C)=10.3650Q$, ($R^2=0.9933$) and $\ln(C_0/C)=10.3916Q$, ($R^2=0.9903$), respectively. Herein, our proposed method demonstrates the usefulness and effectiveness of contaminants degradation as well as monitoring their real-time process of catalytic reaction. Compared with traditional chromatographic and spectroscopic analysis, our sensing system has outstanding advantages of being more portable, sensitive, and intuitional, and has potential application prospects in environmental and electrochemical analysis. This work could be applied in the fields of environmental water treatment, environmental analysis and monitoring, affording a systematic introduction and pioneering technique for environmental catalysis and analytical monitoring.

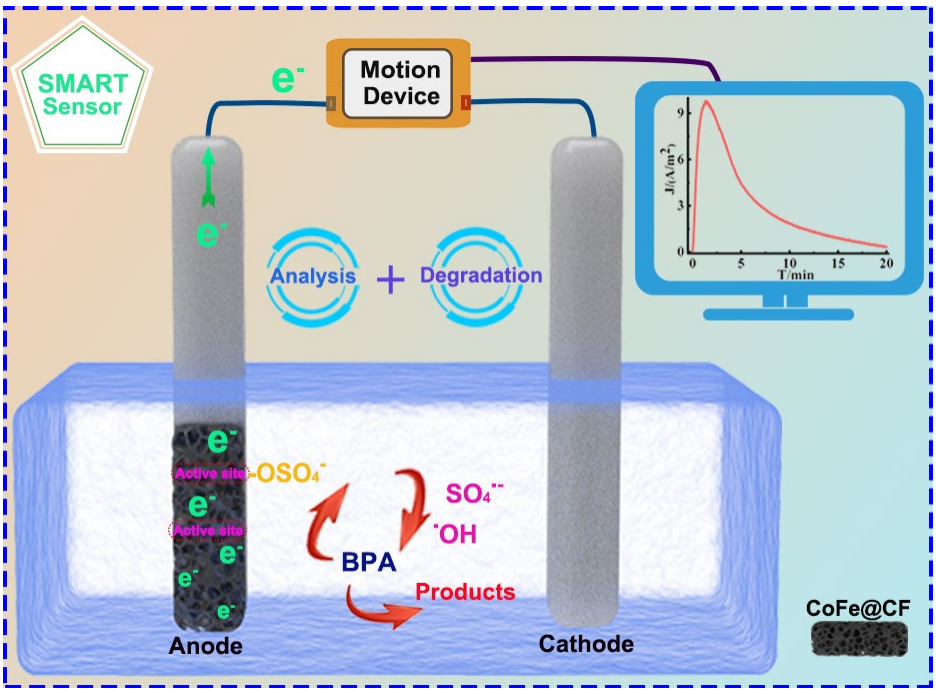

Fig. 1. Application mechanism of the primary cell system with CoFe@CF and graphite carbon as the anode and cathode electrode, respectively.

Experimental part

Reagents and instruments

Bisphenol A, aureomycin, tetracycline, peroxymonosulfate (PMS), methanol, ethanol, polyacrylonitrile (PAN), N, N-dimethylformamide (DMF), anhydrous sodium sulfate (Na_2SO_4) and polyvinylidene fluoride (PVDF) were purchased from Sinopharm Group Chemical Reagent Co., Ltd. 2-methylimidazole (HMIM), cobalt nitrate and ferric nitrate were purchased from Shanghai Aladdin Biochemical Technology Co., Ltd.

Material Preparation

Preparation of Co-ZIFs: 0.35 g of 2-methylimidazole (HMIM) was dissolved in 2 mL of N, N-dimethylformamide (DMF), denoted as solution A. Then 0.8 g of $Co(NO_3)_2$ was dissolved in DMF (1 mL), and recorded as solution B. Rapidly mix solutions A and B and stir for 30 min to obtain Co-ZIFs. After that, 0.2 g of polyacrylonitrile (PAN) was added at 600 rpm stirring speed and completely dissolved after 20 min.

Preparation of FeCo-ZIFs: Solution A: 0.35 g of 2-methylimidazole (HMIM) was dissolved in 2 mL of DMF. Solution B: 0.8 g of $Co(NO_3)_2$ was mixed with different (0.05 g, 0.1 g, 0.2 g and 0.3 g) of $Fe(NO_3)_3$ in DMF (1 mL). Rapidly mix solutions A

and B and sonicate for 10 min to obtain FeCo-ZIFs. After the reaction for 30 min, 0.2 g PAN was added and stirred at 600 rpm for 20 min to obtain FeCo-ZIFs products with different ratios.

Preparation of blank carbon fiber (CF): 0.8 g of fiber paper was calcined at 700 °C under N_2 atmosphere. The resulting product was ground into the CF powder.

Preparation of Co@CF and FeCo@CF: The resulting Co-ZIFs and FeCo-ZIFs solution were covered on fiber paper and placed in an oven for 12 h. The dried powder was calcined at 700 °C under N_2 atmosphere. After that, it was ground uniformly to form Co@CF and FeCo@CF powder.

Electrode preparation and modification

Preparation of the modified negative electrode: 100 mg of (C, Co@CF, FeCo@CF powder) was dispersed in 1 mL of anhydrous ethanol, 10 μL of PVDF was added and ultrasonically dispersed for 30 min to form a homogeneous ink. 200 μL of the resulting ink was added dropwise on the graphite electrode plate (2 *2 cm) and dried in an oven at 50 ℃ for 12 h to obtain (C, Co@CF, FeCo@CF) negative electrode.

Catalytic performance evaluation

Measure 20 mL certain concentrations of BPA, aureomycin or tetracycline, 20 mL of deionized water through a graduated cylinder, add into a quartz beaker and stir thoroughly at 400 rpm. 0.568g of Na_2SO_4 was weighed into the solution and dissolved it uniformly to obtain salt-containing wastewater. A series of electrodes were systematically evaluated by measuring the degradation performance. The catalyst-modified electrodes and carbon electrodes were inserted into the contaminant solution and connected through wires. After the current was stabilized, the sensitive ammeter was zeroed and timed. At regular intervals, a small amount of the reaction solution was collected into the centrifuge tube with the methanol solution for radical bursting. The dynamic concentration of contaminants was analyzed by ultraviolet spectrophotometer and high-performance liquid chromatography (HPLC). In this experiment, the current generated during degradation is collected by an in situ current detector. The voltage is measured by using a sensitive voltmeter.

First-principles calculations

The spin-polarized first-principles calculations have been conducted using density-functional theory based the Vienna Ab initio Simulation Package (VASP.5.4.4.18) with the projector augmented wave method generated pseudopotential and Perdew-Burke-Ernzerhof exchange-correlation functional. To understand the interaction between PMS and nitrogen doped graphene with two different substrates (Co and FeCo), we have constructed two interface models as shown in Figure 7, in which a vacuum layer with 15 Å thickness has been applied. The cutoff energy for electronic plane-wave expansion was set to 400 eV, and the first-Brillouin zone was sampled by Γ centered 6×6×1 *k*-point meshes. For the PMS adsorption, we used DFT-D3 method to consider the van der Waals effect. The adsorption energy was calculated by using below equation:

$$E_a = E_{PMS+Sub} - (E_{PMS} + E_{Sub}),$$

where $E_{PMS+Sub}$, E_{PMS}, and E_{Sub} are the total energy of the interface models, the isolated PMS and the substrates, respectively.

Results and discussion

The FeCo@CF catalysts were constructed by loading carbon fiber (CF) with bimetallic ZIFs and following thermal treatment. Scanning electron microscope (SEM) and transmission electron microscope (TEM) were conducted to investigate their structures. It can be seen that the FeCo@CF is lamellar structure (shown in Fig. 2a), the morphological changes of CF before coating with FeCo can be clearly seen in Fig. S1, which is smoother compared with the FeCo@CF. Regular nanoparticles were observed on the CF surface by high magnification SEM shown in Fig. 2b. TEM (Fig. 2c) of FeCo@CF verified the average size of nanoparticles was about 10 nm. Further detailed the structure information was obtained by high-resolution TEM (Fig. 2d) images. The crystal structure was measured with a lattice spacing distance of 2.00 Å, which is in consistence with the (200) facet of FeCo alloy. The elemental components of the FeCo@CF were examined by energy dispersive spectroscopy (EDS), the composition of the elements Co, Fe, C, N and O in FeCo@CF is observed in Figure

2(d-e), where the ratio of Co to Fe is close to 4:1.

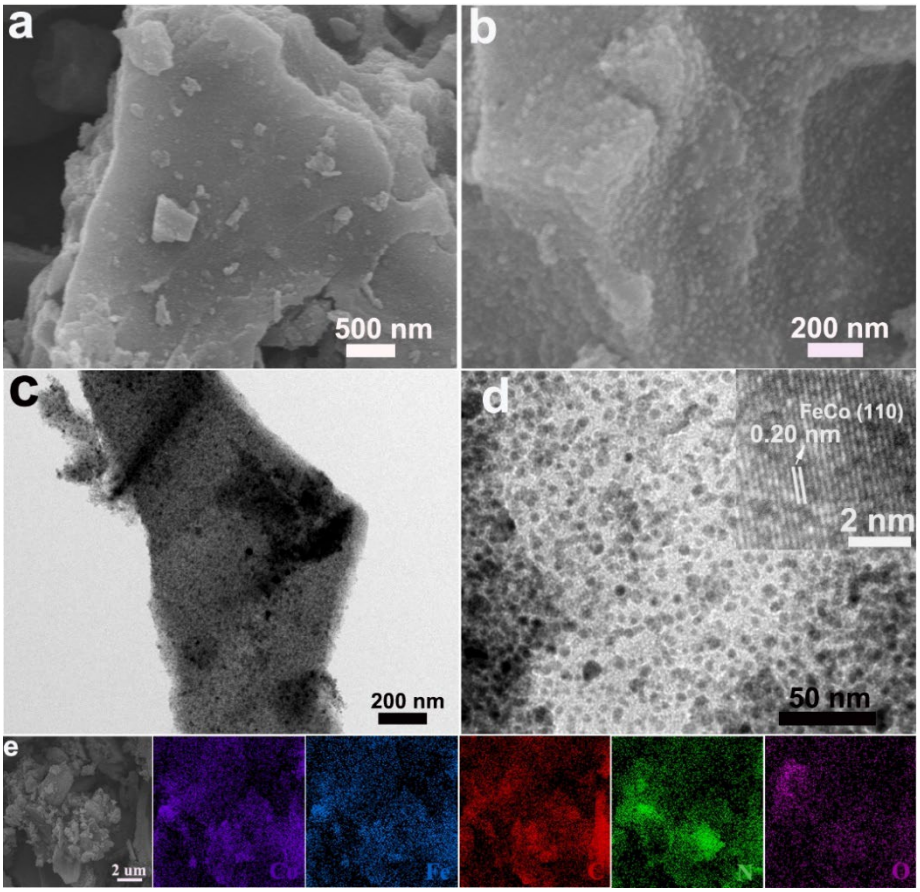

Fig. 2 (a, b) SEM, (c) TEM and (d) HRTEM images of FeCo@CF, Elemental mapping of FeCo@CF in Co, Fe, C, N and O, respectively.

To understand the crystal structure of the obtained catalytic materials, systematic investigations of the X-ray diffraction (XRD) pattern were carried out. As shown in Fig. 3a, the XRD pattern of CF possesses characteristic peaks at 26.2°, which can be indexed by the (002) diffractions of graphite carbon. The XRD pattern of Co@CF exhibited well-defined peaks at 44.2°, 51.5° and 75.9°, corresponding to (111), (200), and (220) planes of Co (PDF No:15-0806), respectively. XRD spectra of the FeCo@CF displays two strong diffraction peaks at 44.8° and 65.3°, which corresponded to the (110) and (200) facets of the FeCo (PDF No:49-1567), respectively. It is proved that the crystal structure of Co@CF changes after adding of Fe. In addition, the (002) diffraction peak of graphitic carbon was found at 26.2° in all the synthesized materials, proving the presence of graphitized carbon in the Co@CF and FeCo@CF. To gain insight into the surface valence states of FeCo@CF, the high-resolution X-ray photoelectron

spectroscopy (XPS) of O 1s, N 1s, Fe 2p and Co 2p are analyzed and shown in Fig.3b-d, respectively. The high-resolution C 1s spectrum in Fig. 3c was deconvoluted into three peaks at 284.6, 285.7, and 288.3 eV, which are related with graphitic carbon, hydroxyl or epoxy groups of carbon, and carbonyl group of carbon, respectively [37-38]. The peak intensity at 284.6 eV is the strongest, which is consistent with sp2 carbon in FeCo@CF. The high-resolution N 1s spectra in Fig. 3d was divided into four peaks at 398.7, 400.5, 401.5 and 405.1 eV, which are associated with Pyridinic N, Pyrrolic, Graphitic N, and Oxidized N, respectively [37-38]. The presence of multiple N species could facilitate enhanced electron transfer and improve the catalytic effect. For the high-resolution XPS spectra of Co 2p (Fig. 3b), two prominent peaks are observed in Co $2p_{1/2}$ and Co $2p_{3/2}$, which can be deconvoluted into Co^0 (780.8 and 795.5 eV), Co^{2+} (780.9 and 797.2 eV), Co^{3+} (782.7 and 798.4 eV), and satellite peaks (786.8 eV and 804.1 eV). The high-resolution Fe 2p spectra in Fig. 3c can be deconvoluted into Fe^0 (707.8 and 720.9 eV), Fe^{2+} (711.3 and 724.3 eV) and satellite peaks (713.9 eV), respectively. The multifarious valence of Fe and Co metal may be due to oxidation of the metal surfaces, which is consistent with the earlier reported FeCo alloy [39-40]. Thus, the presence of zero-valent state metals was verified and the successful synthesis of FeCo@CF.

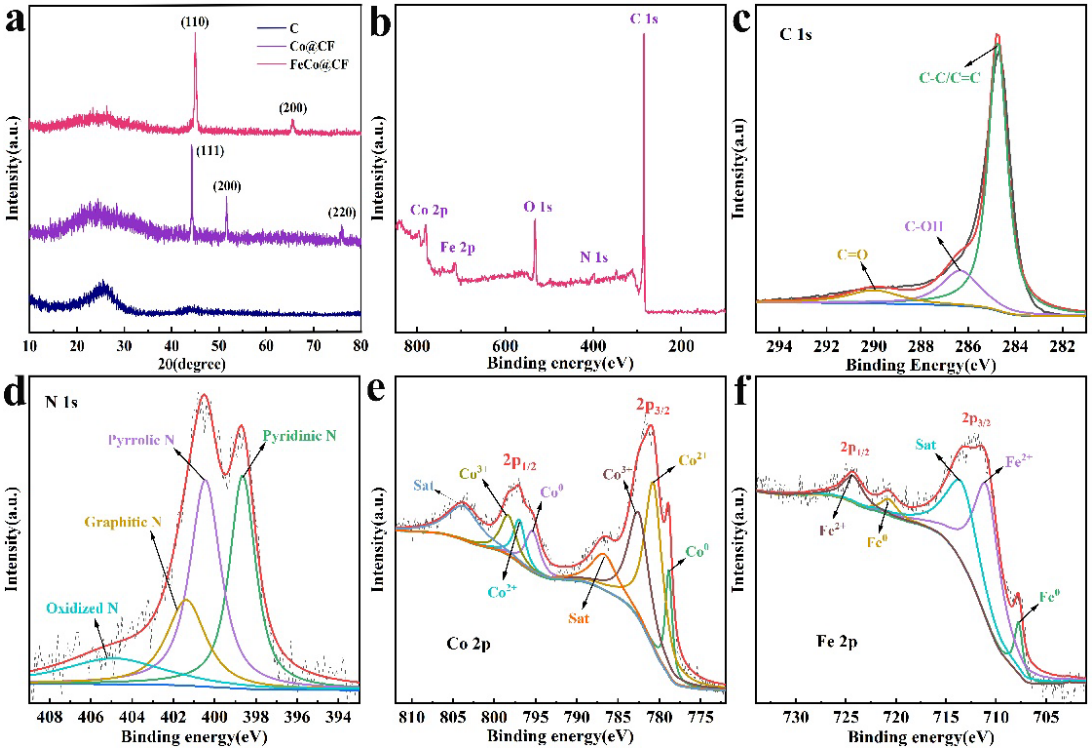

Fig. 3 (a) XRD of C, Co@CF, FeCo@CF, (b) Full spectrum and high-resolution (c) C 1s, (d) N 1s, (e) Co 2p, (f) Fe 2p XPS spectrum of FeCo@CF.

Optimize experimental conditions

The degradation and monitoring system was constructed with graphite plate filled C, Co@CF, or FeCo@CF electrodes used as the negative electrode and the graphite plate electrodes used as the positive electrodes, respectively. The degradation of BPA and corresponding electrochemical signals were compared, as shown in Fig. 4. FeCo@CF showed a greater advantage in degradation performance than Co@CF, while the C electrode had almost no degradation effect on BPA (Fig. 4a). When the catalytic reaction time was 20 min, the removal BPA rates of C, Co@CF and FeCo@CF electrodes were calculated as 8.2%, 69.6% and 96.8%, respectively. To determine their transferred electrons, an innovative method was used to monitor the generated current during the degradation according to the principle of the primary cell, as shown in Fig. 4b. It can be seen that the current densities of Co@CF and FeCo@CF increase rapidly at the beginning and reaches the maximum values at 0.7 min (4.2 A/m^2), 1.3 min (9.8 A/m^2), respectively, after which the current density gradually decreased until no change occurs at 20 min. Interestingly, the current density of the C remained almost constant with little curve fluctuation, the maximum current density of CF was 0.3 A/m^2. The

results showed that the current densities from C, Co@CF to FeCo@CF electrodes were increased sequentially. The real-time voltage of the different electrodes is also tested by in-situ means during the degradation. From the Fig. 4c, we can see that the voltage increases rapidly in the first 4 min of the catalytic reaction, and the rising rate of the voltage tends to level off as the catalytic time is prolonged. By comparing C, Co@CF to FeCo@CF electrodes, we find that the C electrode produces the smallest voltage, Co@CF electrode the second, and FeCo@CF electrodes have the highest timing voltages. To further determine the catalytic oxidation capacity of different electrodes, the real-time electric power of C, Co@CF and FeCo@CF was introduced using the formula of P=UI based on the real-time output voltage, as shown in Fig. 4d, the highest electric power of C, Co@CF and FeCo@CF electrodes were 0.02 mW (20 min), 0.41 mW (0.7 min) and 1.1 mW (2 min), respectively. The power density curves were integrated and average power densities were calculated as 0.060, 1.07 and 2.00 W/m^2 for C, Co@CF, and FeCo@CF, respectively. The charge of the electrodes is related to the electron transfer capacity and which can be calculated as 0.72 C, 0.42 C and 0.05 C for C, Co@CF, and FeCo@CF electrodes in 20 min according to the equation of $Q=\int I_t dt$ (Fig. 4e). The ratio of the number of electrons transferred can also be calculated for C, Co@CF, and FeCo@CF electrodes as 0.07:0.52:1. Moreover, cyclic voltammetry (CV) curves curves of C, Co@CF, and FeCo@CF electrodes were compared in a 0.1 M Na_2SO_4 solution at the scan rate of 50 mV s^{-1}. As shown in Fig. 4f, C electrode exhibited the smallest CV closed curve, while the CV curve of the Co@CF electrode is larger with pseudocapacitance characteristic. The largest closure curve is found at the FeCo@CF electrode, and the pseudocapacitance is more distinctive. Herein, The FeCo@CF electrode exhibits stronger catalytic oxidation capability, faster response to current density, and more effective BPA degradation than other modified electrodes, which may be due to the highest redox activity during the degradation of BPA. The subsequent studies were mainly based on FeCo@CF electrode for optimization analysis.

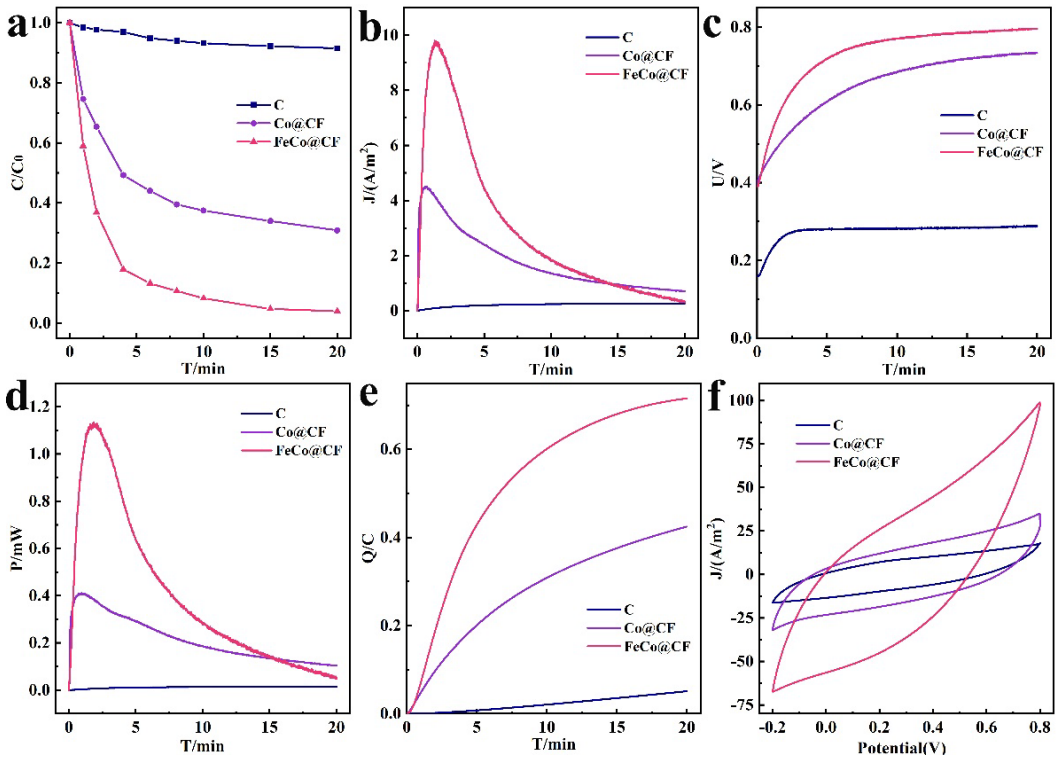

Fig. 4 (a) Degradation effect of C, Co@CF, FeCo@CF electrode on BPA, (b) current density-time, (c) electric power-time, (d) electric power-time (e) charge-time and (f) CV curves of C, Co@CF, FeCo@CF electrode.

Effect of the performance of FeCo@CF

Considering the effect of masses of catalyst, the relationship between the loading of FeCo@CF (5, 10 and 15 mg/cm^2) and the degradation of BPA were compared by covering an electrode area of 2 × 1 cm^2, as shown in Figure S1a, at 20 min, the degradation of BPA was significantly reduced by the 5 mg/cm^2 FeCo@CF electrode compared to the 10 mg/cm^2 electrode, which may be due to the insufficient active site for effective activation of PMS. The degradation of BPA also decreased slightly when the loading of FeCo@CF catalyst was 15 mg/cm^2. This is due to a higher catalyst loading increasing the thickness of the electrode, in which case there is no complete contact between the contaminants and the catalysts, resulting in the reduced degradation of BPA. Catalytic experiments showed that the catalyst loading of 5, 10 and 15 mg/cm^2 achieved 77.1%, 96.8% and 91.8% degradation of BPA within 20 min, respectively. The effect of current density was considered in Fig. S1b. The current densities of 5, 10, and 15 mg/cm^2 reached their highest points of 6.8, 9.8 and 8.9 A/m^2 at 0.7 1.4 and 1.3

min, respectively, confirming the maximum current density for 10 mg/cm^2 loading. The electric power curves for different FeCo@CF loadings were exhibited in Figure S1c. The average power density of 5, 10 and 15 mg/cm^2 FeCo@CF loading were calculated to be 0.38, 2.00 and 0.75 W/m^2, respectively. It is thus clear that the catalytic oxidation ability with the loading of 10 mg/cm^2 is the strongest. The real-time variation of the charge is compared in Figure S1d, the charge for 5, 10 and 15 mg/cm^2 electrodes reached to be 0.46 C 0.55 C and 0.72 C at 20 min, respectively. All these results confirm that FeCo@CF loading at 10 mg/cm^2 exhibits superior degradation and electrochemical activity compared to other electrodes.

To further confirm the effect of the FeCo@CF working electrode area, three different loading areas of 1×1, 2×1 and 2×2 cm^2 were tested for the degradation of BPA with a constant (20 mg) mass of FeCo@CF, as shown in Fig. S2a. After 10 min of catalytic reaction, the degradation effects of BPA in the 1×1, 2×1 and 2×2 cm^2 loading areas were 88.0%, 91.7% and 98.0%, respectively. It can be seen that the degradation of BPA increases with the increase of loading area, which may be attributed to the increases of the contact area between the contaminants and catalysts. To investigate electron transfer ability during the catalytic process, we also measured their current densities separately, as shown in Fig. S2b. The current density of 1×1, 2×1 and 2×2 cm^2 loading areas increased rapidly in a short period of time 5.7 A/m^2 (1.3 min), 9.8 A/m^2 (1.4 min) and 13.3 A/m^2 (0.8 min), respectively, followed by a rapid decline. It is concluded that the larger the load area of the working electrode, the greater the electron transfer was generated. Their average power densities were calculated by the electric power curves as 1.03, 2.00, and 2.25 W/m^2, respectively (Fig. S2c). Moreover, their average electrode area output power was 0.79, 0.71 and 0.40C at 20 min, respectively (Fig. S2d). Considering the current stability and additional economy factors, 2×1 cm^2 was selected as the load area for the subsequent experiments.

To determine the effect of positive electrode areas, different (25%, 50% and 100%) positive electrode area was compared while keeping the FeCo@CF electrode constant (2×1 cm^2). As shown in Fig. S3a. The reduction of the positive electrode area reduced

the degradation performance of BPA, about 96.8% of BPA was degraded at 20 min when the area of negative electrode was equal to the graphite electrode, and the percentage decreased to 86.3% and 80.4% when the positive electrode area was 50% and 25% of the original area, respectively. Similarly, the current density was also affected by the graphite area, the highest point of current density decreased from 1.4 min (9.8 A/m^2), 1.0 min (6.4 A/m^2) to 0.8 min (3.5 A/m^2) when the positive area was a decrease from 100%, 50% to 25%, respectively (Fig. S3b). It can be seen that the reduction of graphite area obstructs electron motion, which reduces the current density and the electrical signal is affected. The average electric power density of 100%, 50% and 25% areas were 2.00, 1.38, and 0.46 W/m^2, respectively (Fig. S3c). As can be seen from the charge curves (Fig. S3d), the graphite electrode is 100%, 50% and 25% of the original electrode, and the charges after 20 min of reaction are 0.72C, 0.48C and 0.17C, respectively. Therefore, we choose a positive area equal to the negative area for the next experiments.

The influence of the electrolyte solution (Na_2SO_4) concentration (0.05 M, 0.1 M and 0.2 M) on the reaction system was studied, the results are shown in Figure S4a. After 20 min of catalytic reaction, the degradation effect of different electrodes all reached more than 93%. Therefore, the results showed that the effect of Na_2SO_4 concentrations on FeCo@CF catalytic performance was not significant. The corresponding current density curves are shown in Figure S4b. In the case of low Na_2SO_4 concentration (0.05 M), the current density decreases slightly, probably because the low salt concentration reduces its conductivity. In contrast, the mutual attraction between ionic bonds affects the migration speed, which in turn leads to a decrease in current density at 0.2 M Na_2SO_4. Overall, the Na_2SO_4 concentrations have little effect on their current density. After that, the corresponding electric powers are calculated respectively, as shown in Fig. S4c. The average power density was 1.31, 2.00, and 2.12 W/m^2 at 0.05 M, 0.1 M, and 0.2 M Na_2SO_4, respectively. It can be seen that the average electric power density is more affected at 0.05 M Na_2SO_4. The relationship between charge and time curves shows that the output power was essentially the same at the salt concentration of 0.1 and 0.2 M, both reaching 0.71 C at 20 min, and the output quantity

of charge was only 0.61 C at 20 min (0.05 M Na_2SO_4) (Fig. S4d). According to the experimental conclusion, 0.1 M was subsequently used as the concentration. All control data are summarized and listed in Table 1.

Table 1. Effects of different reaction conditions on electrochemical parameters and BPA degradation. (LM: Loading mass, LA: Loading area, PA: Positive electrode area, ACD: Average current density, APD: Average power density)

C_{Na2SO4} (M)	*Reaction Conditions*								D_{20}(%)
	LM (mg/cm^2)	**LA (cm^2)**	**PA (cm^2)**	**ACD (A/m^2)**	**APD (W/m^2)**	**Q_{20} (C)**	**Σ (ms/cm)**	**C_{PMS} (g/L)**	
0.10	5	2×1	3×2	1.03	0.38	0.46	11.49	0.50	77.1
0.10	**10**	**2×1**	**3×2**	**2.98**	**2.00**	**0.72**	**11.49**	**0.50**	**96.8**
0.10	15	2×1	3×2	1.67	0.75	0.55	11.49	0.50	91.8
0.10	10	1×1	3×2	1.67	1.02	0.40	11.49	0.50	88.0
0.10	10	2×2	3×2	3.29	2.25	0.79	11.49	0.50	97.9
0.10	10	2×1	3×0.5	0.71	0.46	0.17	11.49	0.50	80.3
0.10	10	2×1	3×1	2.02	1.38	0.48	11.49	0.50	86.3
0.05	10	2×1	3×2	2.55	1.31	0.61	6.88	0.50	96.8
0.20	10	2×1	3×2	2.97	2.12	0.71	19.62	0.50	95.8
0.10	10	2×1	3×2	1.54	0.79	0.37	11.49	0.25	70.5
0.10	10	2×1	3×2	4.68	3.48	1.12	11.49	0.75	98.8

Different PMS dosage (0.25, 0.5, and 0.75 g/L) was studied and shown in Figure 5a, it is fact that the PMS dosing was positively correlated with BPA degradation, the higher the dosage of PMS, the faster the degradation efficiency. After degradation for 10 min, the degradation performance of BPA reached 97.9%, 91.7% and 68.8% for 0.75, 0.5, and 0.25 g/L PMS, respectively. The PMS dosing was also related to the current density (Figure 5b), The current density peaks for 0.75, 0.5, and 0.25 g/L PMS was 11.9 A/m^2 (1.5 min), 9.8 A/m^2 (1.4 min) and 8.5 A/m^2 (1.0 min), respectively. This is due to the number of reactive oxygen species involved in the redox reaction increasing with the amount of PMS, resulting in more electron transfer during the reaction. The

electrical power is measured and compared in Fig. 5c. The average power densities for 0.25, 0.5, and 0.75 g/L PMS were 0.79, 2.00, and 3.48 W/m^2, and this result is consistent with the current density. The increase in electron transfers also led to an increase in the charge, as shown in Figure 5d. The charge reached 1.12, 0.72 and 0.37C from 0.25, 0.5 to 0.75 g/L at 20 min. Herein, 0.50 g/L PMS was chosen as the following reaction condition.

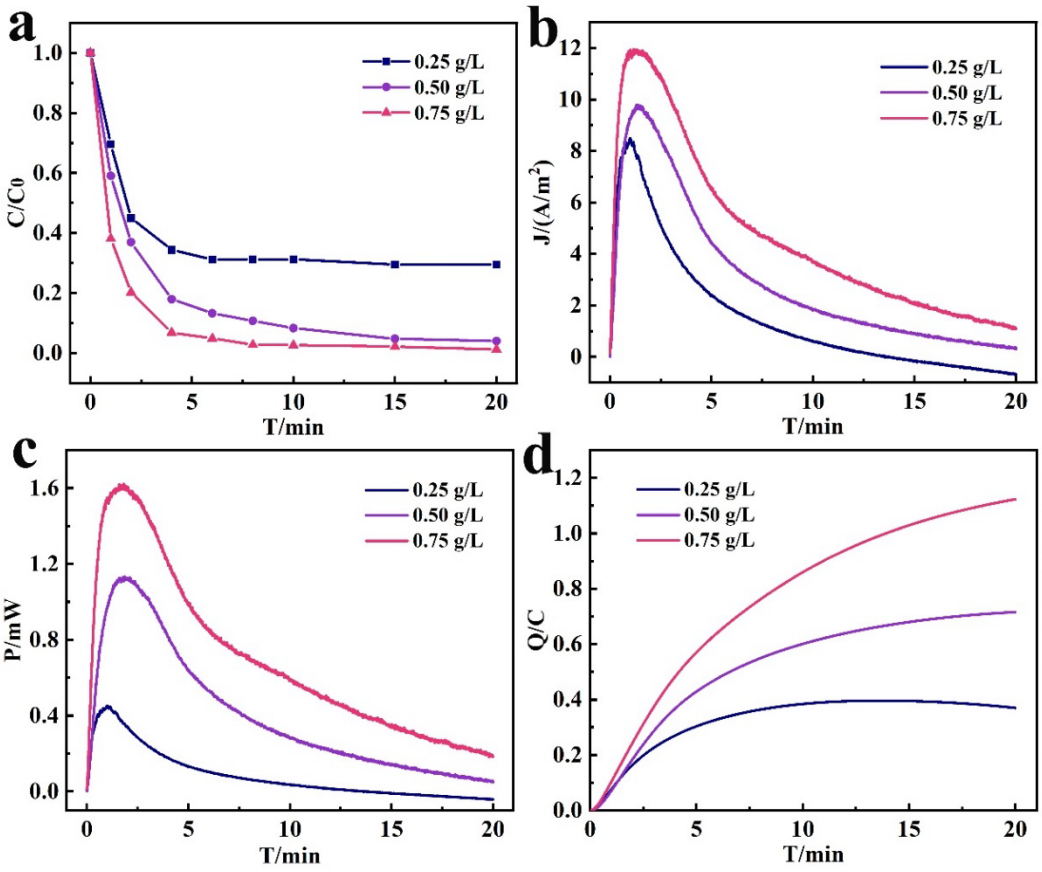

Fig. 5 (a) BPA degradation effect, (b) current densities, (c) electric power (d) quantity of electric charge curves of 0.25, 0.5, and 0.75 g/L PMS.

The degradation performance of BPA was tested by three-dimensional excitation-emission matrix fluorescence spectroscopy. Fig. 6a-d is the contour profiles of BPA degradation at 0, 2, 4 and 8 min, respectively. The upper blue curves and the right red curve on each image correspond to the intensity of the cross-sectional profiles on the contour chart for the blue and red lines, respectively. As can be seen from the figure 6a, there are two fluorescence peaks in BPA concentration at 10 ppm, and the fluorescence intensity reached 1086 (Ex=227 nm, Em=305 nm) and 825.5 (Ex=275 nm, Em=305 nm), respectively. As the reaction proceeded for 2 & 4 min, At the same excitation and

emission wavelength, the contaminant profile intensity gradually decreased from 621.7 and 437.5 to 313.7 and 227.1. In the 8 min catalytic reaction, the fluorescence peak intensity decreased to 44 and 52.23, respectively. The fluorescence intensity of BPA decreased with the decrease of catalytic time, indicating that the FeCo@CF electrode could realize the efficient degradation and conversion of BPA. In comparison with the standard concentration of BPA (Fig.S5), the fluorescence peak was not shifted, indicating that there was no transfer of contaminants during the degradation of BPA.

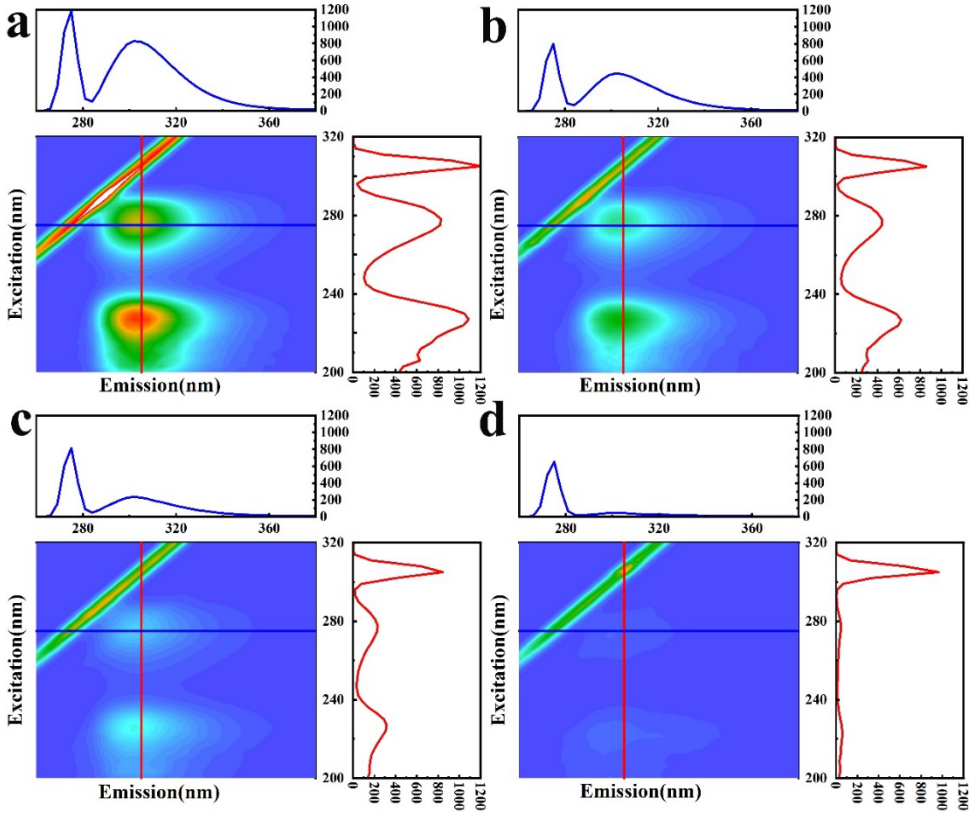

Fig. 6 3D fluorescence contour profiles of the BPA solution at 0 (a), 2 (b), 4 (c) and 8 min (d) of the reaction, respectively.

Density functional theory (DFT) calculations are used to predict the adsorption properties of PMS molecules on the catalyst's configuration. As shown in Fig 7, the adsorption between PMS on the graphene(G)/Co model is exhibited in Figure 7a, and the adsorption of the PMS/G/FeCo model is shown in Figure 7b. It can be seen that the adsorption energy of PMS/G/Co substitution sites is -2.79 eV, while the PMS/G/FeCo interacts more strongly with an adsorption energy of -3.39 eV. The charge density redistribution of PMS/G/FeCo (Fig. 7d) and PMS/G/FeCo (Fig. 7e) is compared, the

green and red-purple denote accumulated and depleted charge density, respectively. We note that when adsorbed PMS on G/FeCo, the charge distribution of the carbon layer changed significantly than PMS/G/Co, revealing the chemisorption of PMS on the G/FeCo substrate. Therefore, the DFT results support our experimental results that the introduction of iron not only enhances the adsorption energy of PMS but also enhances the electron transfer between the configuration structures, leading to the high catalytic activity of the PMS/G/FeCo catalyst.

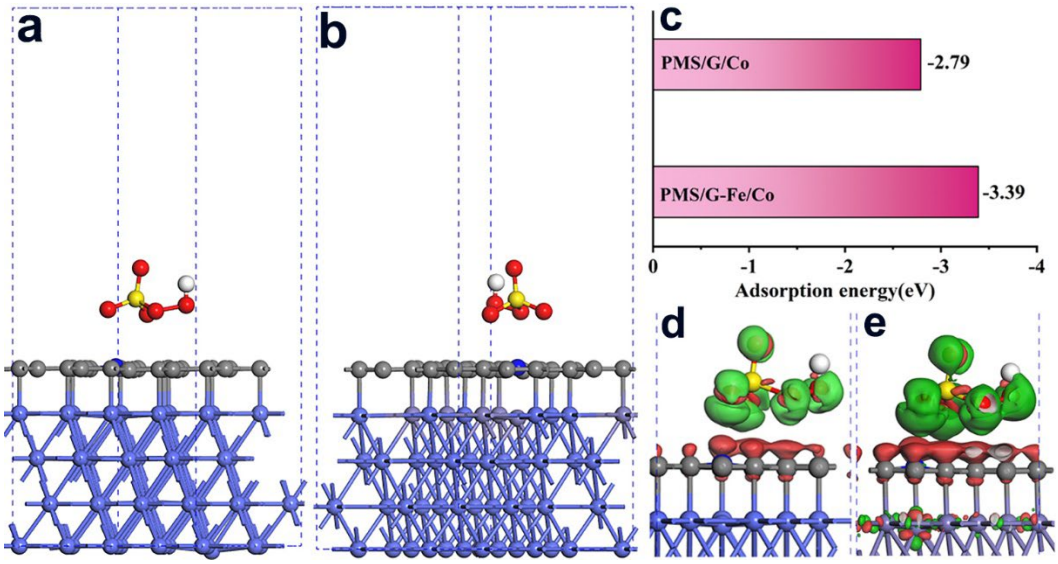

Figure 7 The adsorption configuration (side view) of PMS on the (a) G-Co and (b) G-FeCo substrate. (c) Comparison of adsorption energy of PMS/G-Co and PMS/G-FeCo. The visualized charge density redistribution of (d) PMS/G-Co and (e) PMS/G-FeCo, respectively, where the red and green color denotes accumulated and depleted charge

The correlation between the BPA degradation and the electrical signal of FeCo@CF electrodes was shown in Figure 8. To construct a link between the degradation of BPA at the FeCo@CF electrode and the electrical signal, in situ two-dimensional kernel density of the current density at the FeCo@CF electrode was first understood. As shown in Figure 8, the current density increases rapidly during the first 1 min, and the kernel density in this region is insignificant. After the current density reached the highest value (9.8 A/m^2) at 1.4 min, the density of the measurement points gradually increased, and the color of the nucleus density changed from light to dark at 1.4~10 min. After 10 min, the current density tends to stabilize and the drop point

density continues to increase in this region, and the corresponding kernel density reaches the maximum at 20 min. Based on this, the curves of real-time charge and degradation were compared, as shown in Fig. 8b. Both the degradation curve and the power curve changed as the reaction proceeded, and the curve generated by the reaction changed from fast to slow, and gradually stabilized after 10 min. This may be because the electricity is generated by the electrons transferred during the degradation process after the formation of the primary cell, and there is a connection between the electricity generated during the reduction reaction at the FeCo@CF electrode and the progress of the chemical reaction. To determine the relationship between charge and degradation, the logarithm of the BPA degradation was found to have a good linear relationship with the charge by fitting the real-time charge to the pollutant concentration. Figure 8c observes that the degradation curve is uniformly distributed on both sides of the fitted curve, showing an excellent overlap of linear concentration, and the equation $\ln(C_0/C) = 4.3925Q$, ($R^2 = 0.9987$) was obtained by calculation.

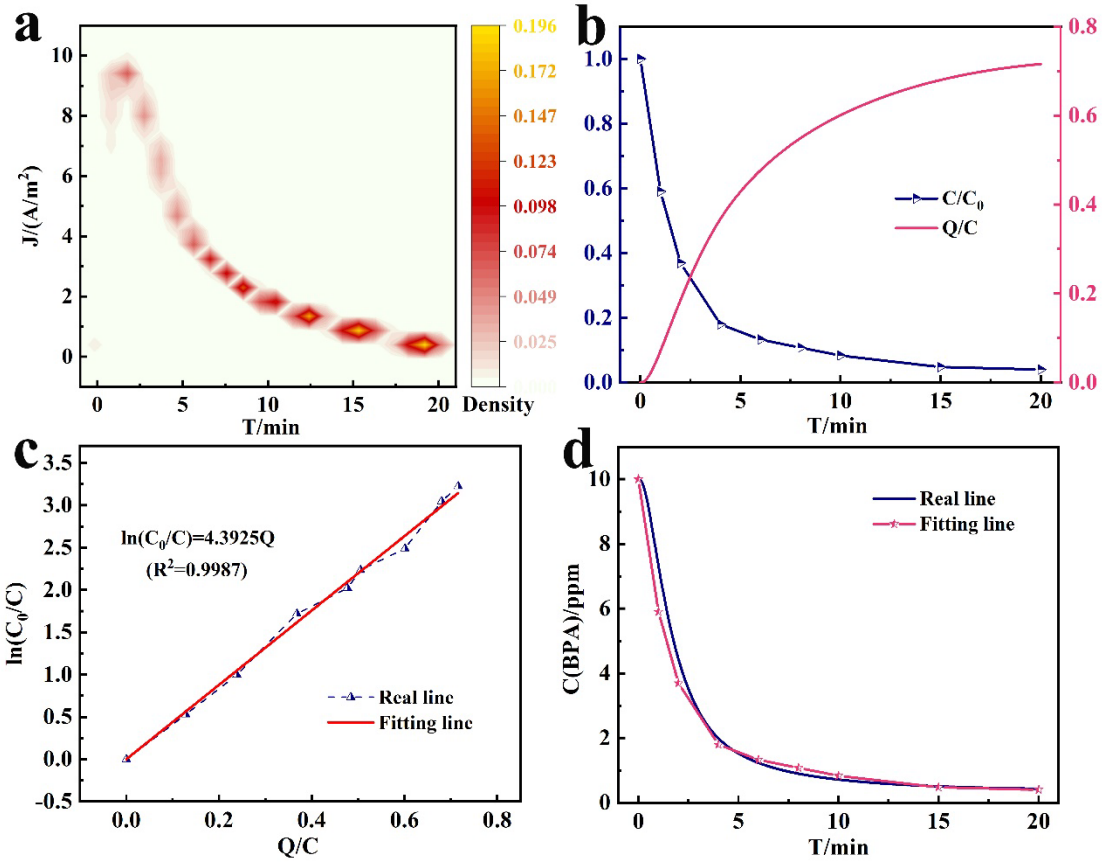

Fig. 8 (a) Two-dimensional kernel density plot of current density, (b) degradation and charge curves, (c) linear fit of ln(C0/C) vs. Q, (d) comparison of simulated and actual degradation curves

of FeCo@CF electrode.

By comparing the theoretical degradation concentration curve to the fitted curve, as shown in Figure 8d. It can be seen that the theoretical degradation curve overlaps with the data of the measured curve, Therefore, the charge-based fit was able to simulate the variation of BPA at each time point. The results highly overlap with the variation of BPA concentration measured by the UV spectrophotometer (Table S1), further confirming the practicality and substitutability of our proposed method. In addition, similar results were obtained by testing the degradation for chlortetracycline and tetracycline, as shown in Fig. S6, kernel density plot of current density for aureomycin and tetracycline degradation proved that the density of the measurement points gradually increased in the catalysis region. A good linear relationship between chlortetracycline and tetracycline degradation with the charge by fitting the real-time charge to the pollutant concentration. The degradation curve shows an excellent overlap of linear concentration, and the equation $\ln(C_0/C)=10.3650Q$, ($R^2=0.9933$) for aureomycin degradation and $\ln(C_0/C)=10.3916Q$, ($R^2=0.9903$) for tetracycline degradation were obtained, respectively. Herein, our constructed sensor exhibits the advantages of being more portable, more sensitive, and visualized than traditional methods. It has extremely prominent and potential applications in the in-situ monitoring of organic pollutant degradation and its concentration.

Conclusion

In this work, a novel bifunctional FeCo@CF negative electrode electrochemical sensor was constructed based on Faraday's effect, which can not only rapidly perform redox reactions with organic pollutants but also set up to measure the current generated during the degradation of organic in situ. The real-time charge (Q) as calculated by the equation of ($Q=zF\xi$), and a good corresponding relationship to the actual measured BPA concentration is calculated as $\ln(C_0/C) =4.3925Q$, ($R^2=0.9987$). Moreover, the Q versus $\ln(C_0/C)$ obtained by measuring tetracycline and chlortetracycline accordingly, which also showed a good linear relationship. Our proposed FeCo@CF sensing electrode are practical and effective in organic degradation as well as monitoring the real-time concentration of pollutants, which exhibited outstanding advantages and potential

application prospects in environmental catalysis and analytical monitoring.